Initiation of In-Plane Shear Instability under Slip-Dependent Friction

by Pascal Favreau, Michel Campillo, and Ioan R. Ionescu

Abstract We study the initiation of an unstable homogeneous elastodynamic in-plane shear process under slip-weakening friction. We assume a linear dependency of the friction at the beginning of the slip, and we make an eigenvalue analysis in the time domain. We prove that two types of eigenvalue are possible. With the first type, the eigenvalues have a negative square and represent the wave part of the solution. With the second type, they have a positive square and lead to the dominant part of the solution. We use a classical method based on the normalization of the dominant eigenfunctions in order to give the analytical expression of the dominant part of the solution. This analysis shows that the response of the dominant part will develop on a continuous but limited spectral domain. This limit depends on the weakening of the friction and a coefficient including the ratio of P-wave velocity to S-wave velocity. We also show that the exponential growth of the dominant part is directly linked to the weakening and the S-wave velocity. Using the expression of the dominant part, we give an estimation of the time of initiation for the crack to reach the steady propagation stage. We perform numerical tests with a finite-difference method and show very good agreement between the analytical dominant part of the solution and the complete numerical solution. Finally, in our case, where the initial stress is equal to the static admissible load, we study the crack propagation and observe that the crack tips travel asymptotically at P-wave velocity after a short time of apparent P supersonic velocity. The numerical results show that the linearized dynamic description is also valid ahead the crack tips in the propagation regime.

Introduction

The initiation stage in dynamic faulting is now considered as a key process in earthquake studies. Perhaps the short time prediction of earthquakes depends on our understanding of this initiation. Ohnaka et al. (1987) and Ohnaka (1996) show in their laboratory experiments that the frictional conditions on the fault during the initiation process can be simply modeled by a slip-dependent friction. Matsu'ura et al. (1992) and Shibazaki and Matsu'ura (1992) proposed a numerical model of earthquake nucleation derived from these experiments. They studied the slip on a specific heterogeneous fault with an external loading. Our goal here is to study separately the dynamic and unstable initiation of the slip at a constant load. This phase takes place between the quasi-static process (where the fault is stable and where the tectonic load is the timescale) and the crack-type propagation (where the waves give the timescale). Campillo and Ionescu (1997) studied theoretically the dynamic evolution of the initiation stage due to a linearized slip-weakening friction in the antiplane case. They calculated an analytical solution for the homogeneous case, and they also gave the time of initiation and the critical length of the perturbations that are able to develop an instability. To complete this work, Ionescu and Campillo (1999) studied

the role of the finiteness of the weak zone at the time of initiation. In the present article, we study the initiation under a homogeneous linearized slip-weakening friction in the in-plane case. Because the method developed by Campillo and Ionescu (1997) for calculating the dominant part of the solution does not apply in the in-plane case, we use another method based on the determination of the eigenfunctions and the calculation of their norm. Finally, we present a quasi-explicit analytical formula of the dominant part. We say quasi-explicit because the formulation needs the numerical calculation of the roots of a high-order polynomial function. Once this little difficulty is solved, one can calculate a theoretical solution. From this analysis, we give the main features of the initiation, and we compare them to the antiplane case. We also perform some simulations with a finite-difference method in order to validate our theoretical expression for the dominant part. Finally, we study the propagation phase of the crack with the finite-difference simulations, and we find that our linearized approach describes well the stress and velocity fields ahead of the crack tips when the admissible static stress is reached everywhere on a large zone of the fault.

1280

Problem Statement

We consider the in-plane shearing of two homogeneous half-spaces bounded by the plane Γ_f at $y = 0$ (see Fig. 1). The half-spaces are in contact with slip-dependent friction. We assume that the displacement field is 0 in the direction z, and we suppose that all our descriptive functions (displacement, stress, and velocity) do not depend on z. The elastic medium has the density ρ and the two wave velocities v_p for P waves and v_s for S waves. The corresponding first Lamé coefficient is $\rho(v_p^2 - 2v_s^2)$, and the second one (the shear modulus) is ρv_s^2. By $\Phi(t,x,y)$ and $\Psi(t,x,y)$, we denote the Helmoltz potentials (corresponding to P and S waves); that is, the displacement u_x, u_y and the stress σ_{xx}, σ_{xy}, σ_{yy} fields can be written as follows:

$$u_x = \frac{\partial \Phi}{\partial x} - \frac{\partial \Psi}{\partial y}, \tag{1}$$

$$u_y = \frac{\partial \Phi}{\partial y} + \frac{\partial \Psi}{\partial x}, \tag{2}$$

$$\sigma_{xx} = \rho v_p^2 \frac{\partial^2 \Phi}{\partial x^2} + \rho(v_p^2 - 2v_s^2)\frac{\partial^2 \Phi}{\partial y^2} - 2\rho v_s^2\frac{\partial^2 \Psi}{\partial x \partial y} + \sigma_{xx}^\infty, \tag{3}$$

$$\sigma_{xy} = \rho v_s^2 \left(2\frac{\partial^2 \Phi}{\partial x \partial y} + \frac{\partial^2 \Psi}{\partial x^2} - \frac{\partial^2 \Psi}{\partial y^2} \right) + \sigma_{xy}^\infty, \tag{4}$$

$$\sigma_{yy} = \rho v_p^2 \frac{\partial^2 \Phi}{\partial y^2} + \rho(v_p^2 - 2v_s^2)\frac{\partial^2 \Phi}{\partial x^2} + 2\rho v_s^2\frac{\partial^2 \Psi}{\partial x \partial y} + \sigma_{yy}^\infty, \tag{5}$$

where σ_{xx}^∞, σ_{xy}^∞, σ_{yy}^∞ is the homogeneous static initial stress field.

The equations of motion, expressed with the potentials, are as follows:

$$\frac{\partial^2 \Phi}{\partial t^2} = v_p^2 \nabla^2 \Phi, \tag{6}$$

$$\frac{\partial^2 \Psi}{\partial t^2} = v_s^2 \nabla^2 \Psi. \tag{7}$$

We assume that the problem has the fundamental symmetry properties $\Phi(t, x, -y) = -\Phi(t, x, y)$ and $\Psi(t, x, -y) = \Psi(t, x, y)$. From these symmetries, we deduce the other useful symmetries $u_x(t, x, -y) = -u_x(t, x, y)$, $u_y(t, x, -y) = u_y(t, x, y)$, $\sigma_{xx}(t, x, -y) + \sigma_{xx}(t, x, y) = 2\sigma_{xx}^\infty$, $\sigma_{xy}(t, x, -y) = \sigma_{xy}(t, x, y)$ and $\sigma_{yy}(t, x, -y) + \sigma_{yy}(t, x, y) = 2\sigma_{yy}^\infty$. The condition of continuity of the stress vector on the fault plane Γ_f gives

$$\sigma_{yy}(t, x, 0^+) = \sigma_{yy}(t, x, 0^-) = \sigma_{yy}^\infty \tag{8}$$

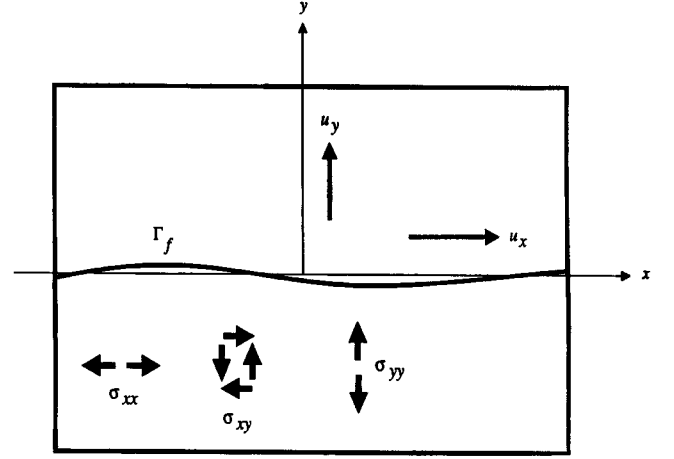$$\sigma_{xy}(t, x, 0^-) = \sigma_{xy}(t, x, 0^+) = \sigma_{xy}(t, x, 0); \tag{9}$$

Figure 1. The in-plane problem. Notations.

that is, the normal stress does not admit any variation during the slip. The condition of symmetry of the normal displacement $u_y(t, x, -y) = u_y(t, x, y)$ already gives its continuity; that is, the crack will not open. The friction boundary condition on the fault plane Γ_f reads

$$\sigma_{xy}(t, x, 0) = -\sigma_{yy}^\infty \mu[x, \delta u_x(t, x)] \operatorname{sign}[\delta v_x(t, x)]$$
$$\text{if } \delta v_x(t, x) \neq 0 \tag{10}$$
$$|\sigma_{xy}(t, x, 0)| \leq -\sigma_{yy}^\infty \mu[x, \delta u_x(t, x)]$$
$$\text{if } \delta v_x(t, x) = 0,$$

where $\delta u(t, x) = u_x(t, x, 0^+) - u_x(t, x, 0^-)$ and $\delta v(t, x) = \dot{u}_x(t, x, 0^+) - \dot{u}_x(t, x, 0^-)$ are the relative slip and the relative slip rate on the fault, and $\mu(x, \delta u)$ is the slip-dependent friction coefficient. The initial conditions

$$u_x(0, x, y) = u_x^0(x, y), \ u_y(0, x, y) = u_y^0(x, y) \tag{11}$$

$$\dot{u}_x(0, x, y) = v_x^0(x, y), \ \dot{u}_y(0, x, y) = v_y^0(x, y) \tag{12}$$

are defined as a small perturbation of the equilibrium and obey the symmetry conditions expressed before. We consider in this article only the case of a homogeneous fault and a friction law with a piecewise linear dependence on the slip (see Fig. 2); that is,

$$\mu(x, \delta u) = \mu_s - \frac{\mu_s - \mu_d}{2L_c} \delta u \quad \text{if } \delta u \leq 2L_c, \tag{13}$$

$$\mu(x, \delta u) = \mu_d \quad \text{if } \delta u > 2L_c. \tag{14}$$

The fault is at the rupture level everywhere at $t = 0$; therefore, $\sigma_{xy}^\infty = -\sigma_{yy}^\infty \mu_s = \sigma_s$, where σ_s is the admissible static stress. The choice of this particular condition is motivated by two reasons. The first one is physical: We want to describe the unstable evolution of the slip near an equilibrium position. Therefore, we must suppose that there ex-
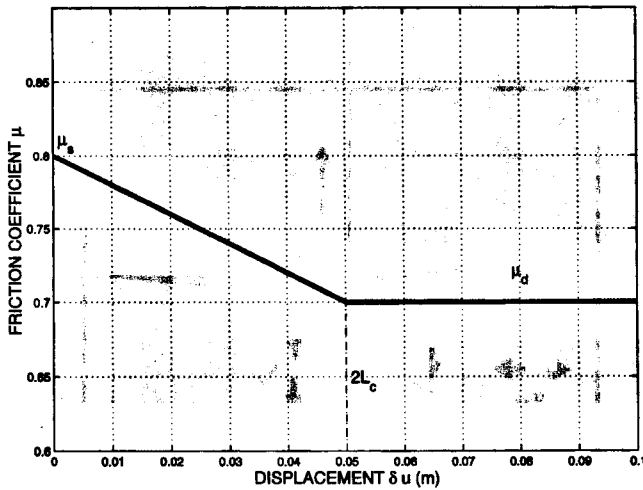
Figure 2. The slip-dependent-friction law. Three parameters μ_s (static friction), μ_d (dynamic friction), and L_c (critical slip) define the idealized slip-dependent-friction law.

ists a large enough zone on the fault where the strength has been reached. The second reason is more technical: We want to perform an eigenvalue analysis, and we want to calculate an analytical dominant part for the slip on the fault. This linearization needs the condition that the strength is reached everywhere on the fault. In practice, the validity of this assumption will be limited to the very beginning of the process. We must point out again that the aim of this work is to give some mathematical features of the homogeneous initiation process, that is, the form of its evolution and its spectral representation. The time of growth is deduced from the response of the system to an initial perturbation that is as small as we want. One easily verifies that if the initial perturbation is zero, that is, $u_x^0(x, y) = 0$, $v_x^0(x, y) = 0$, $u_y^0(x, y) = 0$, and $v_y^0(x, y) = 0$, then $u_x(t, x, y) = 0$ and $u_y(t, x, y) = 0$ are solutions of our problem. Finally, the complete symmetry of our equations gives us the possibility to consider only the half-space $y \geqq 0$. To complete the notations, we denote by $\sigma_d = -\sigma_{yy}^\infty \mu_d$ the ordinary dynamic stress.

Eigenvalue Problem

Our goal is to write the solution for the initiation phase in a spectral form. By definition, the initiation phase corresponds to the stage when the slip is less than $2L_c$ at all the points of the fault (see equation 13). In this particular domain, we rewrite the friction condition in this way:

$$\frac{\sigma_{xy}(t, x, 0)}{\rho v_s^2} = -\alpha_c u_x(t, x, 0), \qquad (15)$$

where

$$\alpha_c = -\sigma_{yy}^\infty \frac{\mu_s - \mu_d}{\rho v_s^2 L_c} = \frac{\sigma_s - \sigma_d}{\rho v_s^2 L_c} \qquad (16)$$

is an important parameter that compares the weakening of the fault to the rigidity of the body.

Because we guess the existence of real positive eigenvalues in the spectral representation of the solution, we want to extract the dominant part of the solution by taking only the eigenfunctions whose time dependence is exponentially growing (real positive eigenvalue) rather than oscillating (imaginary eigenvalue) (see Campillo and Ionescu, 1997). By λ, we denote the eigenvalue, and by $\Phi^\lambda(x, y)$ and $\Psi^\lambda(x, y)$, the eigenfunctions for the potentials. The eigenvalue problem is summarized by

$$\lambda^2 \Phi^\lambda(x, y) = v_p^2 \nabla^2 \Phi^\lambda(x, y), \quad y > 0, \qquad (17)$$

$$\lambda^2 \Psi^\lambda(x, y) = v_s^2 \nabla^2 \Psi^\lambda(x, y), \quad y > 0, \qquad (18)$$

$$\eta^2 \frac{\partial^2 \Psi^\lambda}{\partial y^2}(x, 0) + (\eta^2 - 2)\frac{\partial^2 \Phi^\lambda}{\partial x^2}(x, 0)$$
$$+ 2 \frac{\partial^2 \Psi^\lambda}{\partial x \partial y}(x, 0) = 0, \qquad (19)$$

$$2 \frac{\partial^2 \Phi^\lambda}{\partial x \partial y}(x, 0) + \frac{\partial^2 \Psi^\lambda}{\partial x^2}(x, 0) - \frac{\partial^2 \Psi^\lambda}{\partial y^2}(x, 0)$$
$$= -\alpha_c \left[\frac{\partial \Phi^\lambda}{\partial x}(x, 0) - \frac{\partial \Psi^\lambda}{\partial y}(x, 0) \right], \qquad (20)$$

where $\eta = v_p/v_s$.

By $u_x^\lambda(x, y)$, and $u_y^\lambda(x, y)$, we denote the corresponding eigenfunctions for the displacement that must be derived from the potentials following equations (1) and (2). Before one begins the eigenvalue analysis, one must know the type of the eigenvalues; that is, are they real, imaginary, or complex numbers? If we remember that the medium is homogeneous, we can demonstrate (see Appendix A) the important relation for two eigenfunctions:

$$\int_{-\infty}^{+\infty} \int_0^{+\infty} \lambda_i^2 [u_x^{\lambda_i}(u_x^{\lambda_j})^* + u_y^{\lambda_i}(u_y^{\lambda_j})^*](x, y)\, dy\, dx$$

$$= \int_{-\infty}^{+\infty} [\alpha_c v_s^2 u_x^{\lambda_i}(u_x^{\lambda_j})^*](x, 0)\, dx \qquad (21)$$

$$- \int_{-\infty}^{+\infty} \int_0^{+\infty} e_d^{\lambda_i,\lambda_j}(x, y)\, dy\, dx$$

Here $e_d^{\lambda_i,\lambda_j}$ is the volumetric strain energy function. Its expression is given in Appendix A. It has the symmetry $e_d^{\lambda_j,\lambda_i} = (e_d^{\lambda_i,\lambda_j})^*$.

By taking $i = j$ in equation (21), we deduce that λ_i^2 is real, and consequently, we have $\lambda \in \mathbb{R}$ or $\lambda \in i\mathbb{R}$.

Using the Fourier transform, we now express the eigenfunctions for the potentials as linear combinations of expo-

nential functions. These eigenfunctions satisfy the eigen-value problem summarized in equations (17) to (20) and the finite-energy conditions at $x = \pm\infty$ and $y = +\infty$. There-fore, the eigenfunctions have the generic form

$$\Phi^\lambda(x, y) = e^{ikx} (P_1 e^{py} + P_2 e^{-py}), \qquad (22)$$

$$\Psi^\lambda(x, y) = e^{ikx}(S_1 e^{sy} + S_2 e^{-sy}), \qquad (23)$$

where k is necessarily real because of the finite-energy con-dition at $x = \pm\infty$. Since λ can be either real or imaginary, it follows from the equations of motion that p and s are also either real or imaginary. Finally P_1, P_2, S_1, and S_2 are com-plex.

After using all the conditions of the problem, we find four types of eigenfunctions (see Appendix B) that comply with them. In the first set, the eigenfunctions are a combi-nation of propagating P and S waves, and they can be pa-rameterized by the two wavenumbers k and s. The other numbers $p = p(k, s)$ and $\lambda = \pm\lambda_I(k, s)$ are deduced from them. In the second set, the eigenfunctions are the combi-nation of S waves and P vanishing waves. They are also parameterized by the two wavenumbers k and s. The num-bers $p = p(k, s)$ and $\lambda = \pm\lambda_{II}(k, s)$ are also deduced from them. In the third set, the eigenfunctions are the combination of P and S vanishing waves, and they are only parameterized by the single wavenumber k. The numbers $s = s(k)$, $p = p(k)$, and $\lambda = \pm\lambda_{III}(k)$ are deduced from it. Finally, in the fourth set, the eigenfunctions are not waves but vanishing and unstable functions. They are parameterized by the single wavenumber k. The numbers $s = s(k)$, $p = p(k)$, and $\lambda = \pm\lambda_{IV}(k)$ are also deduced from it. The fourth set of eigen-functions is the base of the dominant part of the solution. As can be seen in this fourth set, there is a limited spectral domain ($|k| < k_c$) in which the instability develops after the initial perturbation. Therefore, large wavenumbers ($|k| > k_c$) do not participate in the unstable growth of the crack. This critical wavenumber k_c is defined by

$$k_c = \frac{\alpha_c}{2(1 - 1/\eta^2)} = \left(\frac{\sigma_s - \sigma_d}{\rho v_s^2 L_c}\right) \frac{1}{2} \left(\frac{v_p^2}{v_p^2 - v_s^2}\right). \qquad (24)$$

We associate the critical half-length of the unstable patch $l_c = \pi/2k_c$, and we find

$$l_c = \left(\frac{\pi \rho v_s^2 L_c}{\sigma_s - \sigma_d}\right) \left(\frac{v_p^2 - v_s^2}{v_p^2}\right). \qquad (25)$$

This exact formula was given by Rice (1980). Andrews (1976) found an analog but slightly different formula by using the Griffith fracture criterion. Das and Aki (1977) de-duced Andrew's formula from Irwin criterion. Both fracture criteria are equivalent to deduce the critical length of growth of a crack (see Aki and Richards, 1980). In our present work, this result is derived from a stability analysis of the dynamic

displacement field that allows us to write down the analytical form of the solution. We give a short demonstration of the existence of the critical wavenumber k_c in Appendix C. Further analysis shows that the maximal real value for the eigenvalue λ is obtained if $k = 0$, then $s(0) = \alpha_c$, $p(0) = \alpha_c/\eta$, and $\lambda(0) = v_s\alpha_c$.

Our conclusion is that the eigenfunctions containing the whole unstable part of the solution can be parameterized by the single real number k with $|k| < k_c$.

Analytical Dominant Part

In this section, our aim is not to write a complete spec-tral formulation of the solution but to extract its dominant part. The dominant part is in fact the truncation of the spec-tral formulation to the fourth set of dominant eigenfunctions written in Appendix B. Because we perform a truncation of the spectrum ($|k| < k_c$), the dominant part does not respect exactly the principle of causality. This question is further discussed in subsequent sections. First, let us return to the property of the causal complete solution (dominant part + wave part) before extracting the dominant part. We classi-cally consider that the complete solution can be written as a linear combination of all the eigenfunctions calculated in the previous section. For example, for the potential $\Phi(t, x, y)$, we obtain

$$\Phi(t, x, y) = \Phi^w(t, x, y) + \Phi^d(t, x, y) \qquad (26)$$

with

$$\Phi^w(t, x, y) = \int_{-\infty}^{+\infty} \int_{-\infty}^{+\infty} [W_{Ia\pm}^{k,s} \Phi_{Ia}^{k,s}(x, y)$$

$$+ W_{Ib\pm}^{k,s} \Phi_{Ib}^{k,s}(x, y)$$

$$+ W_{Ic\pm}^{k,s} \Phi_{Ic}^{k,s}(x, y)]e^{\pm\lambda_I(k,s)t} \, ds \, dk \qquad (27)$$

$$+ \int_{-\infty}^{+\infty} \int_{-|k|\sqrt{(\eta^2-1)}}^{|k|\sqrt{(\eta^2-1)}} W_{II\pm}^{k,s} \Phi_{II}^{k,s}(x, y)e^{\pm\lambda_{II}(k,s)t} \, ds \, dk$$

$$+ \left(\int_{-\infty}^{-k_c} + \int_{k_c}^{+\infty}\right) W_{III\pm}^{k} \Phi_{III}^{k}(x, y)e^{\pm\lambda_{III}(k)t} \, dk$$

and

$$\Phi^d(t, x, y) = \int_{-k_c}^{k_c} W_{IV\pm}^{k} \Phi_{IV}^{k}(x, y)e^{\pm\lambda_{IV}(k)t} \, dk. \qquad (28)$$

The problem is to know the coefficients of the combi-nation precisely. If the eigenfunctions have a property of orthogonality, one can identify each coefficient of the com-bination as the projection of the initial conditions on each corresponding eigenfunction. As we can see in Appendix A,

such an orthogonality exists in our problem by taking ($i \neq j$) in equation (21). This orthogonality property reads

$$\int_{-\infty}^{+\infty} \int_{0}^{+\infty} [u_x^{\lambda i}(u_x^{\lambda j})^* + u_y^{\lambda i}(u_y^{\lambda j})^*](x, y) \, dy \, dx = 0. \quad (29)$$

Finally, to write the dominant part, we just need to calculate the coefficients related to the dominant eigenfunctions, that is, $W_{IV\pm}^k$.

To simplify the formulas, let us write the dominant part for the displacements in this more convenient form:

$$u_x^d(x, y, t) = \int_{-k_c}^{k_c} u_x^k(y)e^{ikx} \left\{ W_0(k)ch[\lambda(k)t] + \frac{W_1(k)}{\lambda(k)}sh[\lambda(k)t] \right\} dk, \quad (30)$$

$$u_y^d(x, y, t) = \int_{-k_c}^{k_c} iu_y^k(y)e^{ikx} \left\{ W_0(k)ch[\lambda(k)t] + \frac{W_1(k)}{\lambda(k)}sh[\lambda(k)t] \right\} dk, \quad (31)$$

where the functions $u_x^k(y)$ and $u_y^k(y)$ are derived in Appendix D from the y dependence of the eigenfunctions $\Phi_{IV}^k(x, y)$ and $\Psi_{IV}^k(x, y)$ (fourth set of Appendix B). In expressions (30) and (31), $W_0(k)$ and $W_1(k)$ replace $W_{IV\pm}^k$, and $\lambda(k)$ replaces $\lambda_{IV}(k)$. Concerning the functions u_x^k and u_y^k, a numerical solution for $s(k)$, $p(k)$, and $\lambda(k)$ is plotted in Figure 3. The numerical value of k_c comes from choices of dimensional quantities given in the next section. The corresponding functions u_x^k, u_y^k are also plotted in Figure 4. To complete the analysis, we give in Appendix D the functions Φ^k and Ψ^k for the

potentials. We also give in Appendix D the stress functions σ_{xx}^k, σ_{xy}^k and σ_{yy}^k and their plots in Figure 4.

We now proceed to the calculation. To obtain $W_0(k)$, we use the initial displacements. First, we write the identity

$$u_x^0(x, y) = u_x^w(0, x, y) + u_x^d(0, x, y)$$
$$= u_x^w(0, x, y) + \int_{-k_c}^{k_c} u_x^k(y)e^{ikx}W_0(k) \, dk, \quad (32)$$

$$u_y^0(x, y) = u_y^w(0, x, y) + u_y^d(0, x, y)$$
$$= u_y^w(0, x, y) + \int_{-k_c}^{k_c} iu_y^k(y)e^{ikx}W_0(k) \, dk, \quad (33)$$

Second, we use the orthogonality property (29) that states that the eigenfunctions constituting the wave part are orthogonal to the one constituting the dominant part. Therefore, the dot product of a dominant eigenfunction of wavenumber k' with the wave part $[u_x^w(0, x, y), u_y^w(0, x, y)]$ at $t = 0$ is zero, that is,

$$\int_{-\infty}^{+\infty} \int_{0}^{+\infty} [u_x^w(0, x, y)u_x^{k'}(y) - iu_y^w(0, x, y)u_y^{k'}(y)]e^{-ik'x} \, dy \, dx = 0. \quad (34)$$

Consequently, the dot product of a dominant eigenfunction of wavenumber k' with the complete solution $[u_x^0(x, y), u_y^0(x, y)]$ at $t = 0$ is reduced to the dot product of this dominant eigenfunction with the dominant part $[u_x^d(0, x, y), u_y^d(0, x, y)]$ at $t = 0$. By replacing $[u_x^d(0, x, y), u_y^d(0, x, y)]$ by its expression in equations (32) and (33), we obtain
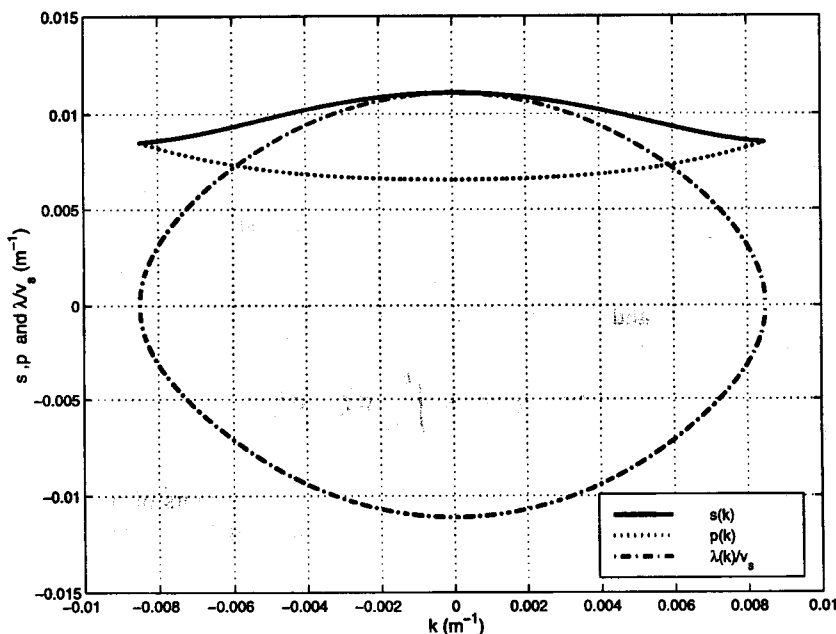

Figure 3. The eigenvalue analysis: the curves $s(k)$, $p(k)$, and $\lambda(k)/v_s$ for $k \in [-k_c, k_c]$ are solved numerically. Their determination allows us to define the dominant eigenfunctions needed for the calculation of the dominant part.
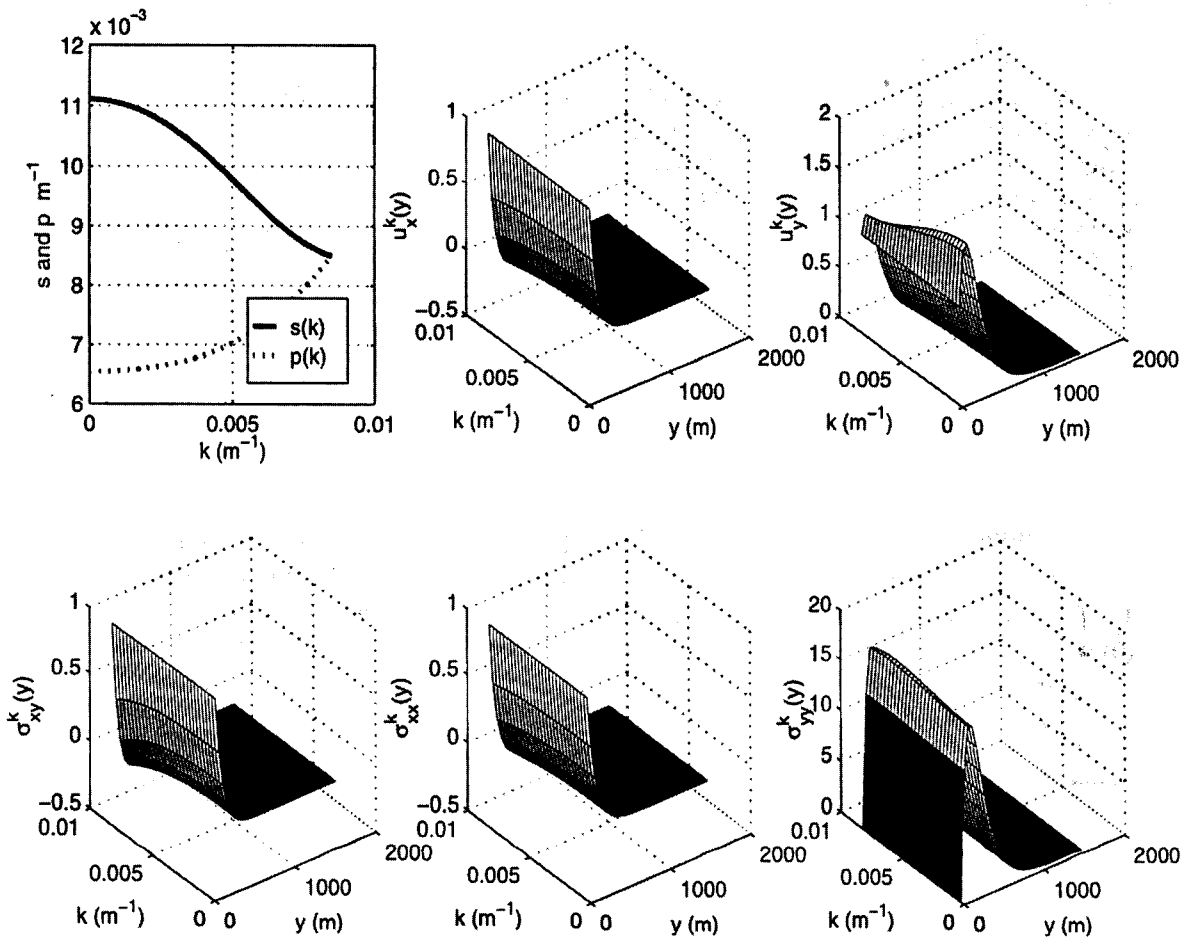
Figure 4. The dominant eigenfunctions. Top left figure, the curves $s(k)$ and $p(k)$ for $k \in [0, k_c]$. The other figures are the representation of the corresponding dominant eigenfunctions for displacements and stresses.

$$\int_{-\infty}^{+\infty} \int_0^{+\infty} [u_x^0(x, y)u_x^{k'}(y) - iu_y^0(x, y)u_y^{k'}(y)]e^{-ik'x} \, dy \, dx$$

$$= \int_{-k_c}^{k_c} \int_{-\infty}^{+\infty} \int_0^{+\infty} [u_x^k(y)u_x^{k'}(y)$$

$$+ u_y^k(y)u_y^{k'}(y)]e^{i(k-k')x}W_0(k) \, dy \, dx \, dk$$

$$= \int_{-k_c}^{k_c} 2\pi\delta(k - k')W_0(k) \int_0^{+\infty} [u_x^k(y)u_x^{k'}(y) \quad (35)$$

$$+ u_y^k(y)u_y^{k'}(y)] \, dy \, dk$$

$$= 2\pi W_0(k') \int_0^{+\infty} [(u_x^{k'})^2(y) + (u_y^{k'})^2(y)] \, dy,$$

where δ is the Dirac function.
The final result is

$$W_0(k) = \frac{1}{D(k)} \int_0^{+\infty} [u_x^k(y)\bar{u}_x^0(k, y)$$

$$- iu_y^k(y)\bar{u}_y^0(k, y)] \, dy, \quad (36)$$

where $\bar{u}_x^0(k, y)$ and $\bar{u}_y^0(k, y)$ are the x-Fourier transforms of the initial displacements and where $D(k)$ is the integral of the square of the eigenfunction components (i.e., their norm):

$$D(k) = \frac{\pi}{s(k)p(k)} (s^2(k)k^2\{4s(k)[k^2 + p^2(k)]$$

$$- 5p(k)[s^2(k) + k^2]\} + p(k)[s^6(k) + k^6]) \quad (37)$$

In the same way, $W_1(k)$ is calculated by replacing the x-Fourier transforms of the initial displacements in equation (36) by the x-Fourier transforms of the initial velocities $\bar{v}_x^0(k, y)$ and $\bar{v}_y^0(k, y)$.

Characteristics of the Initiation Phase

Let us now recall precisely our definition of the initiation phase. It begins at $t = 0$ and ends at the critical time $t = T_c$. For $t < T_c$, every point is on the linear decreasing part of the friction law; that is, $\forall x \ \delta u_x(x, t) \leq 2L_c$. For $t >$

T_c, the crack is in the propagative regime and $[\exists x/\delta u_x(x, t) > 2L_c]$. We consider a small perturbation of u_x and v_x with the support $[-a, a] \times [0, +\infty]$. To determine T_c, we use a simplified expression of the dominant part (30) by considering that the evolution of the displacement is mainly determined by the eigenfunction with the greatest eigenvalue $\lambda(k = 0) = v_s\alpha_c$. Therefore, during the nucleation phase, the solution grows by a factor e in an interval of time $1/(v_s a_c)$. The total time of nucleation depends on the ratio of displacement at the end of nucleation $2L_c$ to the displacement of the projection of the initial perturbation onto the most dominant eigenfunction. For this purpose, we use the foregoing solution with $k = 0$. This approximation is valid if the spectrum of the perturbation is quasi constant on $[-k_c, k_c]$, that is, if $\pi/ak_c \gg 1$. Therefore, for a perturbation of u_x, we have

$$\tilde{u}_x^0(k, y) \approx \tilde{u}_x^0(0, y) = \int_{-a}^{a} u_x^0(x, y)\,dx, \qquad (38)$$

$$W_0(0) = \frac{1}{D(0)} \int_0^{+\infty} [u_x^0(y)\tilde{u}_x^0(0, y)]\,dy$$

$$= \frac{\alpha_c^2}{\pi} \int_0^{+\infty} \int_{-a}^{a} u_x^0(x, y)e^{-\alpha_c y}\,dx\,dy. \qquad (39)$$

The same computation can be done for a perturbation of v_x to obtain $W_1(0)$. If the critical time T_c is large enough, that is, $\lambda(0)T_c \gg 1$, that is, $T_c \gg 1/v_s\alpha_c$, we obtain

$$u_x^d(T_c, 0, 0) \approx k_c u_x^0(0) \left[W_0(0) + \frac{W_1(0)}{v_s\alpha_c}\right] \frac{e^{\lambda(0)T_c}}{2}$$

$$= k_c\alpha_c^3 \left[W_0(0) + \frac{W_1(0)}{v_s\alpha_c}\right] \frac{e^{v_s\alpha_c T_c}}{2}. \qquad (40)$$

The equation $u_x^d(T_c, 0, 0) = L_c$ leads to the following estimation of T_c:

$$T_c \approx \frac{1}{v_s\alpha_c} \ln\left\{\frac{\pi L_c}{\dfrac{2\pi a^2 k_c}{\alpha_c}\left[W_0(0) + \dfrac{W_1(0)}{v_s\alpha_c}\right]}\right\}. \qquad (41)$$

We perform a series of numerical experiments in order to confront the theoretical results for the dominant part with the complete solution calculated with a finite-difference method. The numerical scheme of the finite-difference method is not explained because the details are beyond the scope of this article. We just indicate that it uses a classical finite-difference scheme (Lax–Wendroff) for the iterations in the body. It has been adapted to the existence of the two-phase velocities of P and S waves. We choose $\Delta l = v_p\Delta t$ for the convergence. On the fault, iterations are calculated by using the integration of the characteristic lines to capture the instability. More details on the numerical aspects are given by Ionescu and Campillo (1999). We use a grid of

1200×600 points in the x, y plane. The parameters of computation are $\Delta l = 5$ m, $\rho = 3000$ kg/m^3, $v_s = 3000$ m/sec, $\eta = v_p/v_s = 1.7$, $\sigma_{yy}^\infty = -150$ M Pa, $\sigma_{xy}^\infty = 120$ M Pa, $\mu_s = 0.8$, $\mu_d = 0.7$, and $L_c = 0.05$ M (if no indications are given). With these values, we obtain $\alpha_c = 0.011$ m^{-1}, $k_c = 0.0085$ m^{-2}, and $l_c = 283$ m. The initial conditions are given by

$$u_x^0(x, y) = 0, \quad u_y^0(x, y) = 0, \qquad (42)$$

$$v_x^0(x, y) = v_0 e^{-x^2/a^2 - y^2/b^2}, \quad v_y^0(x, y) = 0, \qquad (43)$$

with always $v_0 = 0.0001$ m/sec and $a = b = 75$ m (if no other indications are given).

In Figure 5, we plot the comparison between the finite-difference method and the dominant part. We observe a very good agreement between these two independent methods. This shows that the unstable evolution of the initiation phase is accurately described by the dominant part. Concerning the evaluation of the time of initiation, we find 0.3777 sec $< T_c < 0.3784$ sec with the finite difference while our approximate formula (41) gives $T_c = 0.3646$ sec.

Rather than to focus on the total time of nucleation, it is also interesting to examine the growth of the perturbation calculated with the finite-difference method. We compute the logarithm of the slip velocity $\log_{10}(\delta v_x(t,0)/\delta v_x(0,0))$ at the center of the perturbation. The results are plotted in Figure 6 for various L_c. The rate of growth associated with the dominant part is given by the slope of the tilted linear part. The beginning of the curves shows the effect of the wave part, whereas the end represents the crack part.

We now want to comment on the similarities and the differences between the antiplane and the in-plane problems. We summarize in Table 1 the main features of the dominant part for both problems.

For the initiation stage, we observe an almost complete similarity between the two problems. The main modification concerns the characteristic length in the in-plane case compared with the antiplane case. Indeed, the in-plane critical length is the antiplane one multiplied by the factor $2(1 - 1/\eta^2)$, that is 1.3 for $\eta = 1.7$. In the in-plane case, the y dependency does not follow the unique exponential function $e^{-\alpha_c y}$ found for the antiplane case but a more complex combination of decreasing exponential functions (see again the dominant eigenfunctions in Fig. 4). In fact, we can consider that the antiplane problem is (mathematically speaking) a particular case of the in-plane problem, where the curve $s(k)$ does not depend on k anymore because in the antiplane case, $s(k) = \alpha_c$ (see Campillo and Ionescu, 1997).

Transition from Initiation to Propagation

Several comments have to be made concerning the physical interpretation of the properties of the initiation phase. To illustrate our purpose, one can see in Figures 7 and 8 the velocity and stress distributions at the particular
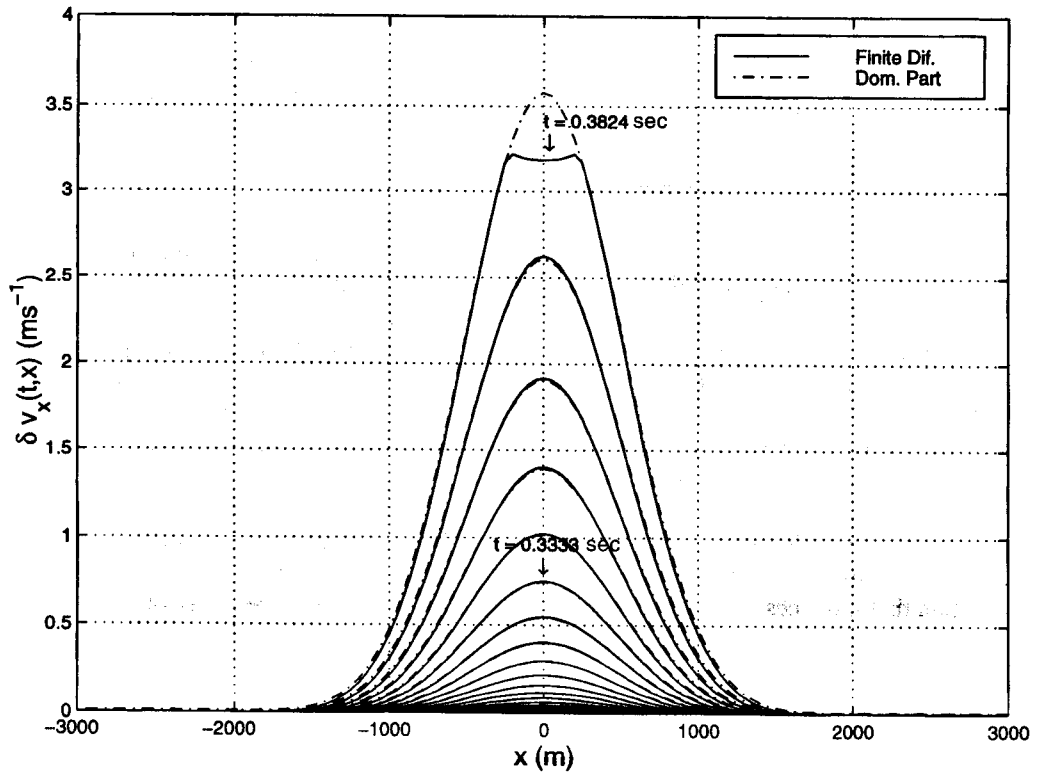
Figure 5. The plot of the velocity on the fault for different times in the initiation phase. See the good agreement between the two independent methods. Let us remark that for the last time, the curve has left the initiation phase.
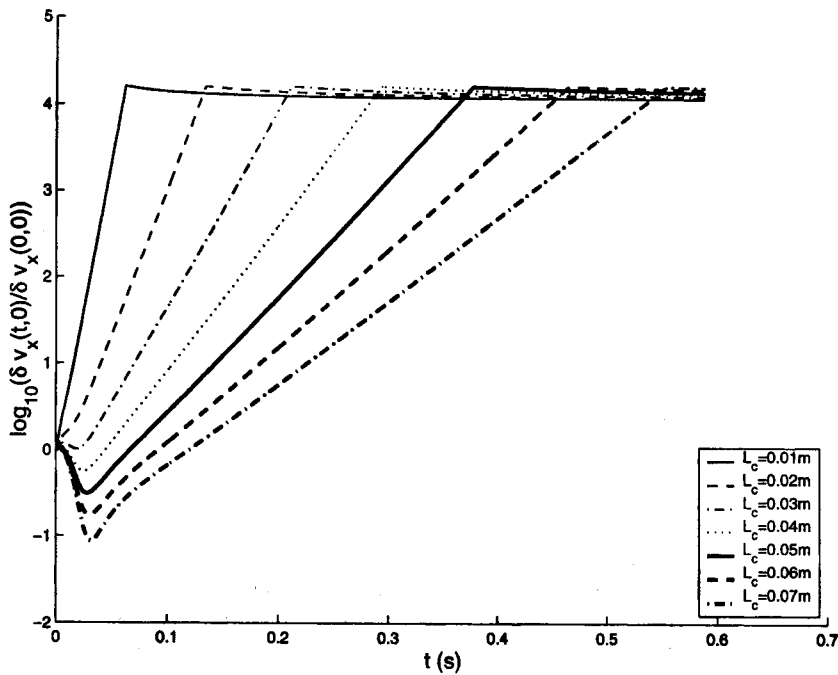

Figure 6. The plot of the logarithm of the velocity for the different values of L_c at the center of the perturbation. For the small values of L_c one can observe the effect of the wave part before the constant rate of growth that corresponds to the dominant part.

Table 1
Main Features of the Antiplane and In-Plane Problems

	Slipping Patch	Time Growth	y Decreasing
Antiplane	π/α_c	$\approx e^{v_s \alpha_c t}$	$e^{-\alpha_c y}$
In-plane	$2(1 - 1/\eta^2)\pi/\alpha_c$	$\approx e^{v_s \alpha_c t}$	$\approx e^{-\alpha_c/\eta\, y}$

time $t_1 = 0.3627$ sec in the initiation phase. First, no singularity is observed for these functions. Indeed, the fault is at the rupture level everywhere, and no stress concentration is possible. Second, the motion evolves globally on the fault, losing the form of the initial perturbation that was only of a size of around 20 grid points. This effect expresses the wavenumber cut at k_c. Third, there is no classical crack tip on the fault. Fourth, there is no visible wave front in the body; that is, the process of initiation is not emitting, and it is localized on the fault. Finally, the meaning of this initiation phase is the nonstationary motion that produces a continuous transi-

tion from the initial perturbation to the propagation of a self-similar crack.

In the following part, without entering in detail in the study of the crack propagation that has been studied by Andrews (1985) in the in-plane case and Virieux and Madariaga (1982) and Day (1982) in three dimensions, we examine the way how the system does the transition between the initiation stage to the propagation stage. Figures 9 and 10 show the velocity and stress functions in the propagative phase at time $t_2 = 0.5882$ sec, computed using the finite-difference method. It is now possible to identify the crack tips and two wave fronts for P and S waves propagating in the body, which indicates a huge radiation compared to the initiation phase. The propagation process is qualitatively very different from the initiation process. Let us now see the relationship between the two stages. In Figure 11, we did three simulations. Curves (1) correspond to the complete simulation of the propagation with finite differences and the friction law represented in Figure 2. Curves (2) are the result of the simulation with finite differences of the initiation phase for a
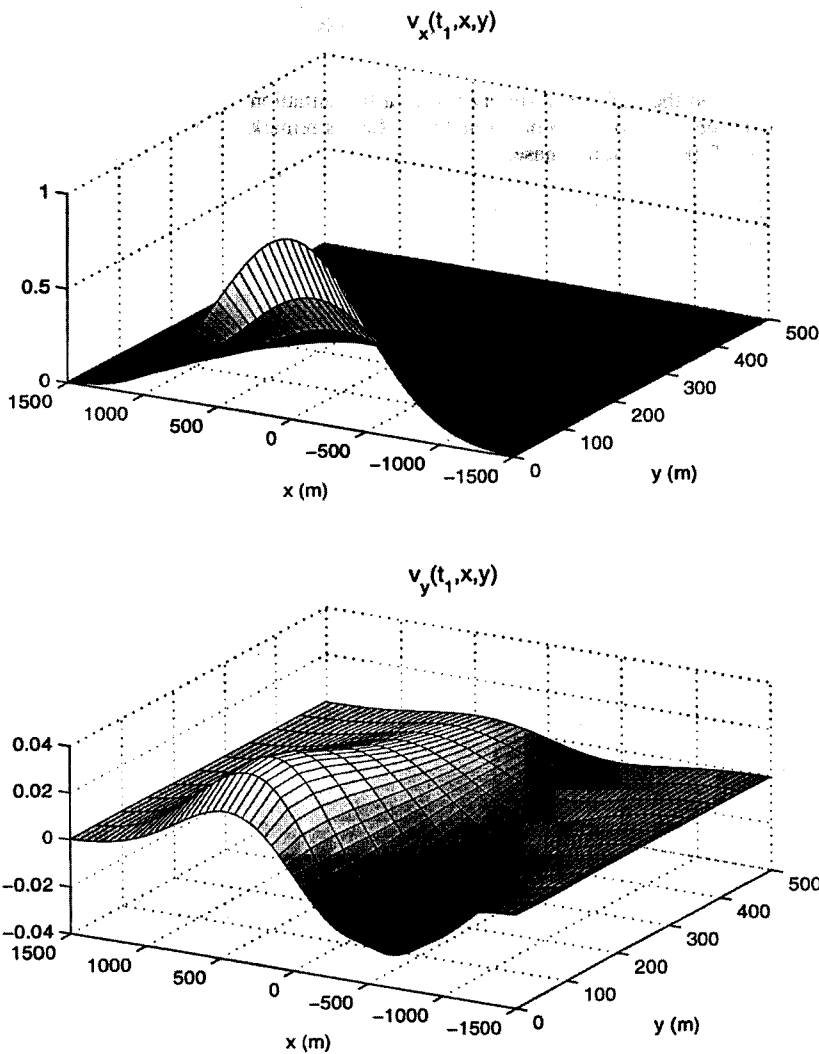

Figure 7. The plot of the velocities in the medium at $t_1 = 0.3627$ sec in the initiation phase. The slip is localized on the fault and no wave is visible.

$\sigma_{xy}(t_1,x,y)$ (MPa)

$\sigma_{xx}(t_1,x,y)$ (MPa)
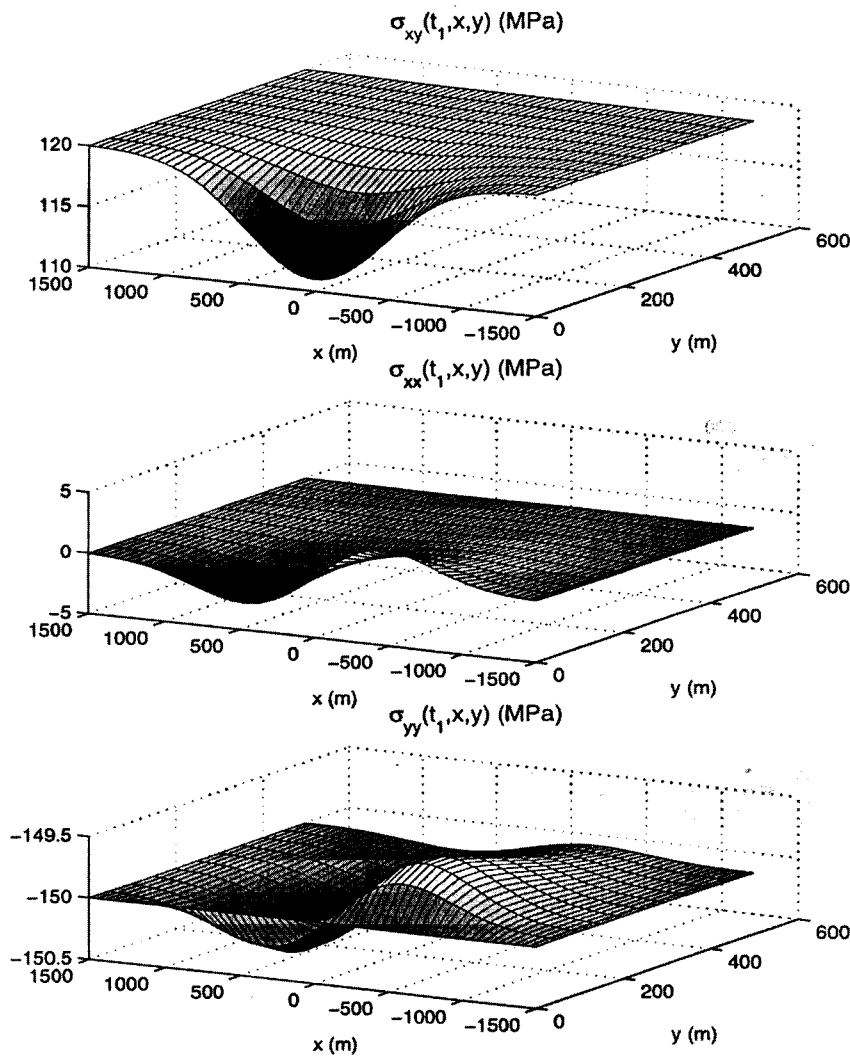
$\sigma_{yy}(t_1,x,y)$ (MPa)

Figure 8.   The plot of the stresses in the medium at $t_1 = 0.3627$ sec in the initiation phase. The stress change is localized on the fault and no wave is visible.

fictitious friction law, in which a constant weakening rate exists whatever the slip; that is, $\sigma_d \to -\infty$, and $L_c \to +\infty$. Curve (2′) is the analytical form of the dominant part extrapolated outside the initiation domain. The dominant part naturally fits with curve (2) when the effect of noncausality (due to a limited spectrum) of (2′) is low (i.e., for small times). For large times, the slip computed is enormous, and the effect of noncausality of the dominant part of the solution can be seen. A striking feature of Figure 11 is that curves (1) and (2) are strictly identical outside the crack zone (by the name *crack zone*, we define the zone inside the crack tips and where the slip exceeds $2L_c$). In fact, this observation shows that the points that have overcome the critical length L_c in the middle of the fault do not disturb the initiation process that continues outside the crack tips, as if all the points outside the crack tips were in a fictive uniform initiation stage. In other words, our linearized approach is still valid ahead the crack tips in the propagation regime. Before giving an explanation to this fact, let us recall the results found by Burridge (1973). He demonstrated that the velocity

of the crack tips of a self-similar crack depends on the parameter $S = (\sigma_s - \sigma_{xy}^\infty)/(\sigma_{xy}^\infty - \sigma_d)$. If $S > 1.63$, the admissible velocity is the Rayleigh wave speed. If $S = 0$, as in our case, the P-wave velocity is admissible. In Figure 12, we plot the trajectory of the crack tips computed with the finite-difference method. These trajectories correspond to curves (1). We observe that the crack tips travel at an apparent velocity larger than the P-wave velocity, but they are always in the cone of causality of the process. After a long time, the crack tip's velocity decreases asymptotically to the P-wave velocity as expected. This observation confirms the results of Burridge, but it also gives us the response to the fact that our linearized approach is valid to describe the velocity and stress fields ahead of the crack tips. Indeed, the crack tips travel at an apparent P supersonic velocity, and therefore, no information from the middle of the fault has enough time to come and perturbate the dynamics of the initiation outside the crack tips. Finally, in this particular case where the fault is near the rupture everywhere, the slip outside the crack tips is well described by the extrapolation
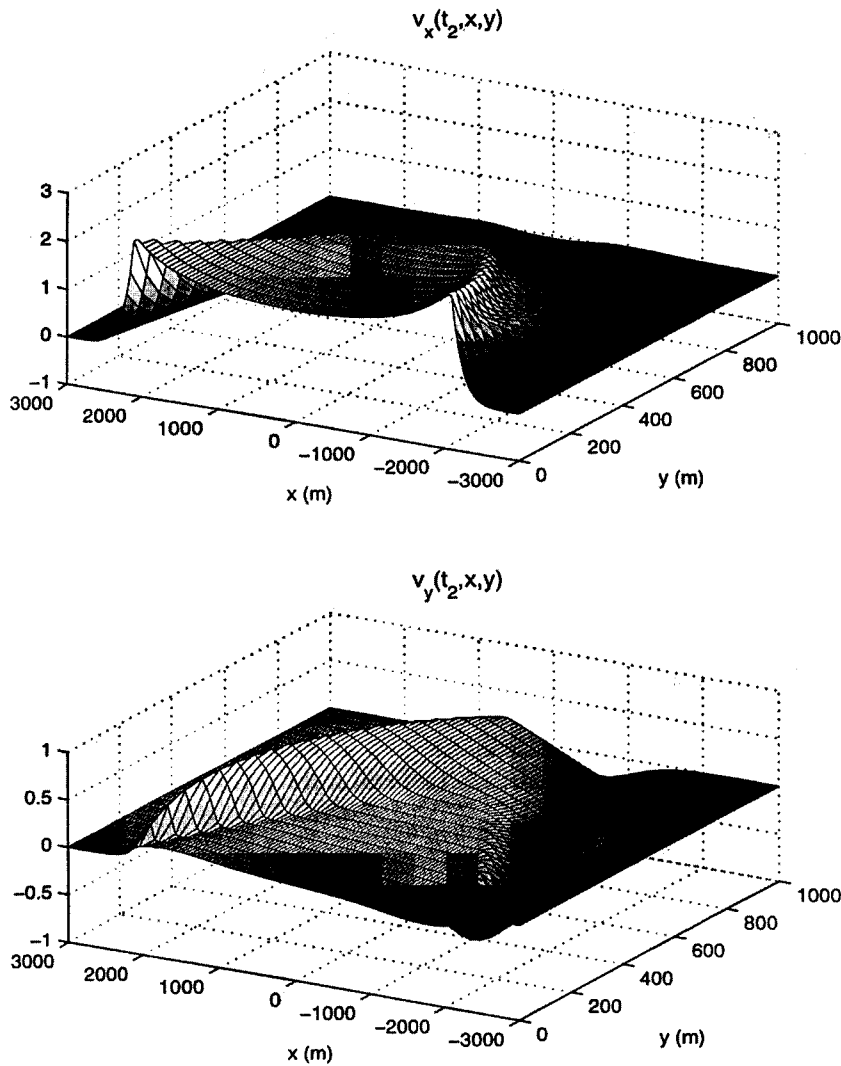
$v_x(t_2,x,y)$

$v_y(t_2,x,y)$

Figure 9. The plot of the velocities in the medium at $t_2 = 0.5882$ sec in the propagation phase. Here the two traveling wave fronts of P and S waves are visible.

of a homogeneous initiation. Our linearized description is still valid to describe it. More precisely, the complete linearized calculation computed with finite difference, corresponding to curves (2), is exact, and the analytical dominant part, corresponding to curves (2'), is valid while its noncausality effect is small, that is, for relatively small times. In another words, the propagation of the crack in our case is not due to the accumulation of stress but is due to the unstable growth of the small perturbation that propagates on the fault at the P-wave velocity, an artifact of the idealization that whole fault is initially at σ_s. In the antiplane case, the same remarks could be done in the same context.

Conclusion

We study the initiation of an unstable in-plane elastodynamic shear crack under slip-weakening friction. Some characteristics were found by previous studies. We propose here an eigenvalue analysis that allows us to define the dom-

inant part of the solution that describes the unstable growth of the slip. We obtain an analytical expression for the dominant part. The formula shows some differences with the antiplane case, but the main features are conserved. Indeed, the unstable part of the response to a little perturbation will develop on a limited spectral domain. The limiting wavenumber (corresponding to the slipping patch) is derived from the slope of the friction law, the shear rigidity, and the ratio between the P- and the S-wave velocities. We also give the characteristic time of growth of the perturbation, which is the same as in the antiplane case. We complete this result by giving an approximation of the time of the initiation phase. Our results are compared to a numerical solution calculated with finite differences. In the propagation regime, we show that the crack tips travel at an apparent P supersonic velocity that tends asymptotically to the P velocity. This observation is in agreement with previous studies in the case where the fault is at the admissible static load everywhere. More than this verification, our simulations gives us an ar-
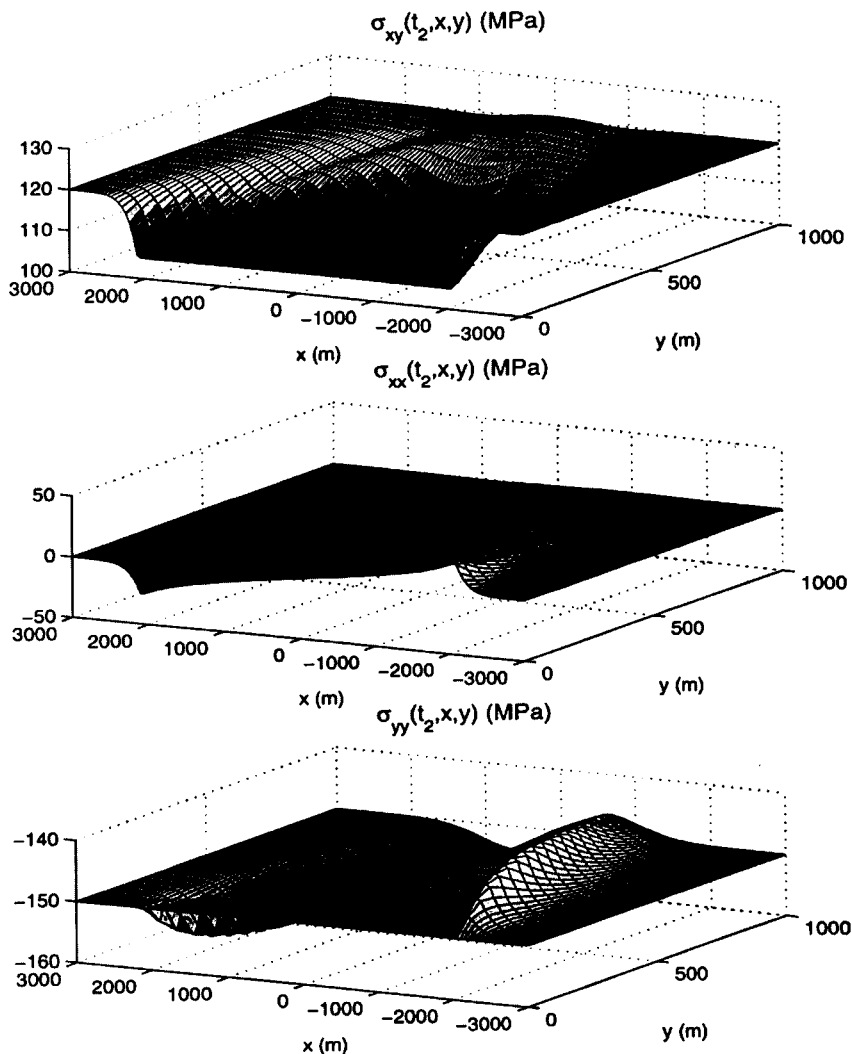
$\sigma_{xy}(t_2, x, y)$ (MPa)

$\sigma_{xx}(t_2, x, y)$ (MPa)

$\sigma_{yy}(t_2, x, y)$ (MPa)

Figure 10. The plot of the stresses in the medium at $t_2 = 0.5882$ sec in the propagation phase. Here the two traveling wave fronts of P and S waves are visible.

gument to say that our linearized approach (for any time) and its description by the dominant part (for short times) is still valid to give the stress and velocity fields ahead of the crack tips in the propagation regime.

Acknowledgments

References

Aki, K., and P. G. Richards (1980). *Quantitative Seismology. Theory and Methods*, W. H. Freeman, New York, 901–911.

Andrews, D. J. (1976). Rupture velocity of plane strain shear cracks, *J. Geophys. Res.* **81**, 5679–5687.

Andrews, D. J. (1985). Dynamic plane-strain shear rupture with a slip-weakening friction law calculated by a boundary integral method, *Bull. Seism. Soc. Am.* **75**, 1–21.

Burridge, R. (1973). Admissible speeds for plane-strain self-similar shear cracks with friction but lacking cohesion, *Geophys. J. R. Astr. Soc.* **35**, 439–455.

Campillo, M., and I. R. Ionescu (1997). Initiation of an antiplane shear instability under slip dependent friction, *J. Geophys. Res.* **102**, 20363–20371.

Das, S., and K. Aki (1977). A numerical study of two-dimensional spontaneous rupture propagation, *Geophys. J. R. Astr. Soc.* **50**, 643–668.

Day, S. M. (1982). Three-dimensional simulation of spontaneous rupture: the effect of nonuniform prestress, *Bull. Seism. Soc. Am.* **72**, 1881–1902.

Ionescu, I. R., and M. Campillo (1999). Numerical study of initiation: influence of non-linearity and fault finiteness, *J. Geophys. Res.* **104**, 3013–3024.

Matsu'ura, M., H. Kataoka, and B. Shibazaki (1992). Slip dependent friction law and nucleation processes in earthquake rupture, *Tectonophysics* **211**, 135–148.

Ohnaka, M. (1996). Non-uniformity of the constitutive law parameter for shear rupture and quasi-static nucleation to dynamic rupture: a physical model of earthquake generation model, *Proc. Natl. Acad. Sci. USA* **93**, 3795–3802.

Ohnaka, M., Y. Kuwahara, and K. Yamamoto (1987). Constitutive relations between dynamic physical parameters near a tip of the propagation slip during stick-slip shear failure, *Tectonophysics* **144**, 109–125.
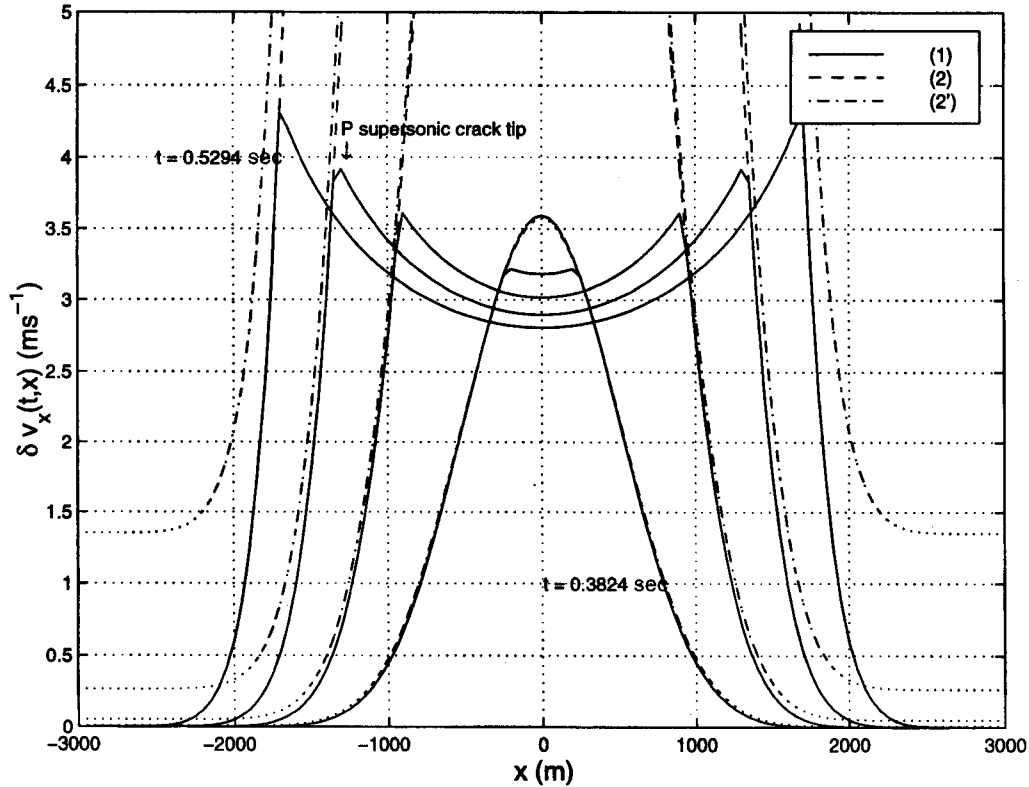
Figure 11. The transition from initiation to propagation. Here we plot the velocity on the fault for different times in the propagation phase. The plot (1) is the simulation in finite difference of the complete solution with a bounding dynamical friction σ_d. The plot (2) is the simulation in finite difference of the initiation as if it could continue without any bounding dynamical friction σ_d. (2') is the analytical dominant part.

Rice, J. R. (1980). The mechanics of earthquake rupture, in *Physics of the Earth's Interiors* A. M. Dziewonski and E. Boschi (Editors), Italian Physical Society/North-Holland, Amsterdam, 555–649.

Shibazaki, B., and M. Matsu'ura (1992). Spontaneous processes for nucleation, dynamic propagation and stop of earthquake rupture, *Geophys. Res. Lett.* **19**, 1189–1192.

Virieux, J., and R. Madariaga (1982). Dynamic faulting studied by a finite difference method, *Bull. Seism. Soc. Am.* **72**, 345–369.

Appendix A

Properties of Eigenvalues and Eigenfunctions

Let us consider an elastic body Ω and its boundary $\partial\Omega$. Let us consider the displacement field u_k and the corresponding stress tensor field σ_{kl}. We write the equation of motion in the body

$$\rho\frac{\partial^2 u_k}{\partial t^2} = \sigma_{kl,l}.$$

We can multiply each side of this equation by any independent field v_k and integrate on the body:

$$\int_\Omega \rho\frac{\partial^2 u_k}{\partial t^2} v_k dV = \int_\Omega \sigma_{kl,l} v_k dV.$$

We consider the equality $\sigma_{kl,l}v_k = (\sigma_{kl}v_k)_{,l} - \sigma_{kl}v_{k,l}$. We recall the symmetry of the stress tensor, that is, $\sigma_{kl} = \sigma_{lk}$, and deduce that $\sigma_{kl}v_{k,l} = \sigma_{kl}\varepsilon_{kl}$, where $\varepsilon_{kl} = (v_{k,l} + v_{l,k})/2$ is the strain tensor associated to the field v_k. We are now able to apply the Gauss theorem, and we find

$$\int_\Omega \rho\frac{\partial^2 u_k}{\partial t^2}v_k dV = \int_{\partial\Omega}\sigma_{kl}v_k dS_l - \int_\Omega \sigma_{kl}\varepsilon_{kl}dV. \quad (A1)$$

We consider the particular case when $u_k = (u_x^{\lambda_i}, u_y^{\lambda_i})$ and $v_k = [(u_x^{\lambda_j})^*, (u_y^{\lambda_j})^*]$. We can replace $\partial^2/\partial t^2$ by $(\lambda_i)^2$ for an eigenfunction. Taking into account the frictional boundary condition (15), we have for our particular problem

$$\int_{-\infty}^{+\infty}\int_0^{+\infty} \lambda_i^2[u_x^{\lambda_i}(u_x^{\lambda_j})^* + u_y^{\lambda_i}(u_y^{\lambda_j})^*](x, y)\, dy\, dx$$

$$= \int_{-\infty}^{+\infty} [\alpha_c v_s^2 u_x^{\lambda_i}(u_x^{\lambda_j})^*](x, 0)\, dx \quad (A2)$$

$$- \int_{-\infty}^{+\infty}\int_0^{+\infty} e_d^{\lambda_i,\lambda_j}(x, y)\, dy\, dx.$$

Here, $e_d^{\lambda_i,\lambda_j} = v_p^2 [\varepsilon_{xx}^{\lambda_i}(\varepsilon_{xx}^{\lambda_j})^* + \varepsilon_{yy}^{\lambda_i}(\varepsilon_{yy}^{\lambda_j})^*] + (v_p^2 - 2v_s^2)$
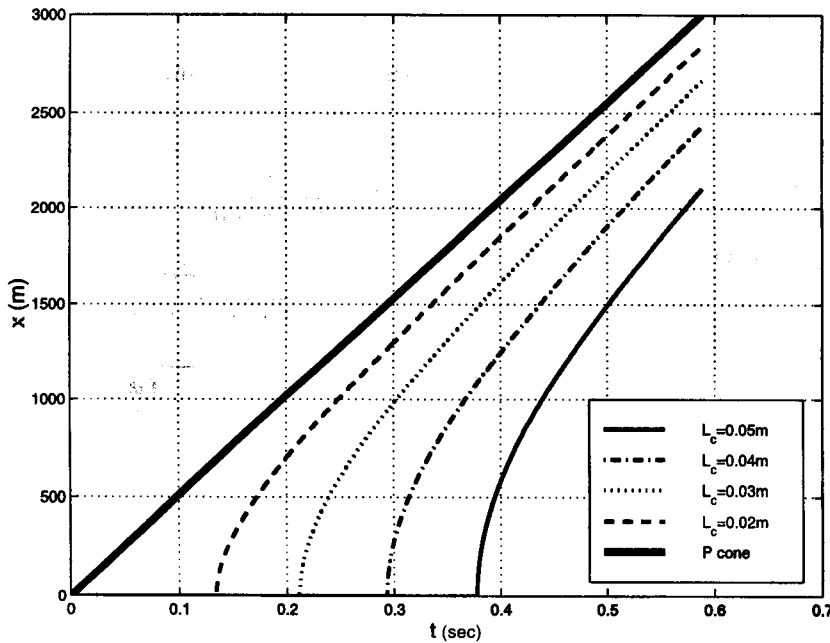
Figure 12. The trajectory of the crack tips on the fault for different values of L_c. Let us see the apparent P-supersonic velocity. It converges asymptotically to the P-wave velocity for great times.

$[\varepsilon_{xx}^{\lambda_i}(\varepsilon_{yy}^{\lambda_j})^* + \varepsilon_{yy}^{\lambda_i}(\varepsilon_{xx}^{\lambda_j})^*] + 2v_s^2\varepsilon_{xy}^{\lambda_i}(\varepsilon_{xy}^{\lambda_j})^*$ is the operator of volumic energy of strain. One can easily remark that it has the symmetry $e_d^{\lambda_j\lambda_i} = (e_d^{\lambda_j\lambda_i})^*$.

If we take $i = j$ in equation (A2), we obtain

$$\lambda_i^2 = \frac{\alpha_c v_s^2 \int_{-\infty}^{+\infty} |u_x^{\lambda_i}|^2(x)dx - \int_{-\infty}^{+\infty}\int_0^{+\infty} e_d^{\lambda_i\lambda_i}(x, y)\, dy\, dx}{\int_{-\infty}^{+\infty}\int_0^{+\infty} (|u_x^{\lambda_i}|^2 + |u_y^{\lambda_i}|^2)(x, y)\, dy\, dx}.$$

(A3)

Because $e_d^{\lambda_j\lambda_i} = (e_d^{\lambda_j\lambda_i})^*$, we deduce that $e_d^{\lambda_j\lambda_i}$ is real and finally that λ_i^2 is real. Consequently, $\lambda_i \in \mathbb{R}$ or $\lambda_i \in i\mathbb{R}$.

Finally, we take the conjugate expression of (A2) and replace i by j, and if we do the difference with (A2), we obtain

$$[\lambda_i^2 - (\lambda_j^2)^*]\int_{-\infty}^{+\infty}\int_0^{+\infty} [u_x^{\lambda_i}(u_x^{\lambda_j})^* + u_y^{\lambda_i}(u_y^{\lambda_j})^*](x, y)\, dy\, dx = 0. \quad (A4)$$

Therefore, if $|\lambda_i| \neq |\lambda_j|$, the integral in equation (A4) is zero, as expected from the property of orthogonality of the eigenfunctions.

Appendix B

The Complete Set of Eigenfunctions

In this section, we denote by η the velocity ratio $\eta = v_p/v_s$.

First Set

In this set, two wavenumbers k and s are needed to describe the eigenfunctions. They have a negative value of λ^2 (stable).

$(k, s) \in \mathbb{R}^2$ with $|s| > |k|\sqrt{(\eta^2 - 1)}$,

$p(k, s) \in \mathbb{R}$ with $p(k, s) = \pm\frac{1}{\eta}\sqrt{s^2 - (\eta^2 - 1)k^2}$,

$\lambda = \pm\lambda_f(k, s) \in i\mathbb{R}$ with $\lambda_f(k, s) = iv_s\sqrt{s^2 + k^2}$,

$\Phi_{Ia}^{k,s}(x, y) = e^{ikx} \{(k^2 - s^2) \sin[p(k, s)y]\}$,

$\Psi_{Ia}^{k,s}(x, y) = e^{ikx} [2ikp(k, s) \cos(sy)]$,

$\Phi_{Ib}^{k,s}(x, y) = e^{ikx} \{4k^2p(k, s) s \cos [p(k, s)y] - \alpha_c s(s^2 + k^2) \sin[p(k, s)y]\}$,

$\Psi_{Ib}^{k,s}(x, y) = e^{ikx} [-2ikp(k, s)(s^2 - k^2) \sin(sy)]$,

$\Phi_{Ic}^{k,s}(x, y) = e^{ikx} \{2iks(s^2 - k^2) \cos[p(k, s)y]\}$,

$\Psi_{Ic}^{k,s}(x, y) = e^{ikx} [\alpha_c s(s^2 + k^2) \cos(sy) + (s^2 - k^2)^2 \sin(sy)]$.

Second Set

In this set, two wavenumbers k and s are needed to describe the eigenfunctions. They have a negative value of λ^2 (stable).

$(k, s) \in \mathbb{R}^2$ with $|s| < |k|\sqrt{(\eta^2 - 1)}$,

$p(k, s) \in \mathbb{R}^+$ with $p(k, s) = \dfrac{1}{\eta}\sqrt{(\eta^2 - 1)k^2 - s^2}$,

$\lambda = \pm\lambda_{II}(k, s) \in i\mathbb{R}$ with $\lambda_{II}(k, s) = iv_s\sqrt{s^2 + k^2}$,

$\Phi_{II}^{k,s}(x, y) = e^{ikx} [2iks(s^2 - k^2)e^{-p(k,s)y}]$,

$\Psi_{II}^{k,s}(x, y) = e^{ikx} \{[\alpha_c s(s^2 + k^2) - 4k^2 p(k, s)s] \cos(sy)$

$\qquad\qquad + (s^2 - k^2)^2 \sin(sy)\}$.

Third Set

In this set, one single wavenumber k is needed to describe the eigenfunctions. They have a negative value of λ^2 (stable).

$k \in \mathbb{R}$ with $|k| > k_c = \dfrac{\alpha_c}{2(1 - 1/\eta^2)}$,

$s(k) \in \mathbb{R}^+$ with $\dfrac{[k^2 + s^2(k)]^2 - \alpha_c s(k)[s^2(k) - k^2]}{4k^2 s(k)}$

$\qquad\qquad = \dfrac{1}{\eta}\sqrt{(\eta^2 - 1)k^2 + s^2(k)}$,

$p(k) \in \mathbb{R}^+$ with $p(k) = \dfrac{1}{\eta}\sqrt{(\eta^2 - 1)k^2 + s^2(k)}$,

$\lambda = \pm\lambda_{III}(k) \in i\mathbb{R}$ with $\lambda_{III}(k) = iv_s\sqrt{k^2 - s^2(k)}$,

$\Phi_{III}^{k}(x, y) = e^{ikx} [2iks(k)e^{-p(k)y}]$,

$\Psi_{III}^{k}(x, y) = e^{ikx} \{[s^2(k) + k^2]e^{-s(k)y}\}$.

Fourth Set

In this set, one single wavenumber k is needed to describe the eigenfunctions. They have a positive value of λ^2 (unstable).

$k \in \mathbb{R}$ with $|k| < k_c = \dfrac{\alpha_c}{2(1 - 1/\eta^2)}$, (B1)

$s(k) \in \mathbb{R}^+$ with $\dfrac{[k^2 + s^2(k)]^2 - \alpha_c s(k)[s^2(k) - k^2]}{4k^2 s(k)}$

$\qquad\qquad = \dfrac{1}{\eta}\sqrt{(\eta^2 - 1)k^2 + s^2(k)}$, (B2)

$p(k) \in \mathbb{R}^+$ with $p(k) = \dfrac{1}{\eta}\sqrt{(\eta^2 - 1)k^2 + s^2(k)}$, (B3)

$\lambda = \pm\lambda_{IV}(k) \in \mathbb{R}$ with $\lambda_{IV}(k) = v_s\sqrt{s^2(k) - k^2}$, (B4)

$\Phi_{IV}^{k}(x, y) = e^{ikx} [2iks(k)e^{-p(k)y}]$, (B5)

$\Psi_{IV}^{k}(x, y) = e^{ikx} \{[s^2(k) + k^2]e^{-s(k)y}\}$. (B6)

Appendix C

Critical Wavenumber k_c

We define the dimensionless functions $\bar{s} = s(k)/k$, $\bar{p} = p(k)/k$, and $\bar{\alpha}_c = \alpha_c/k$, and we rewrite equations (B2) and (B3):
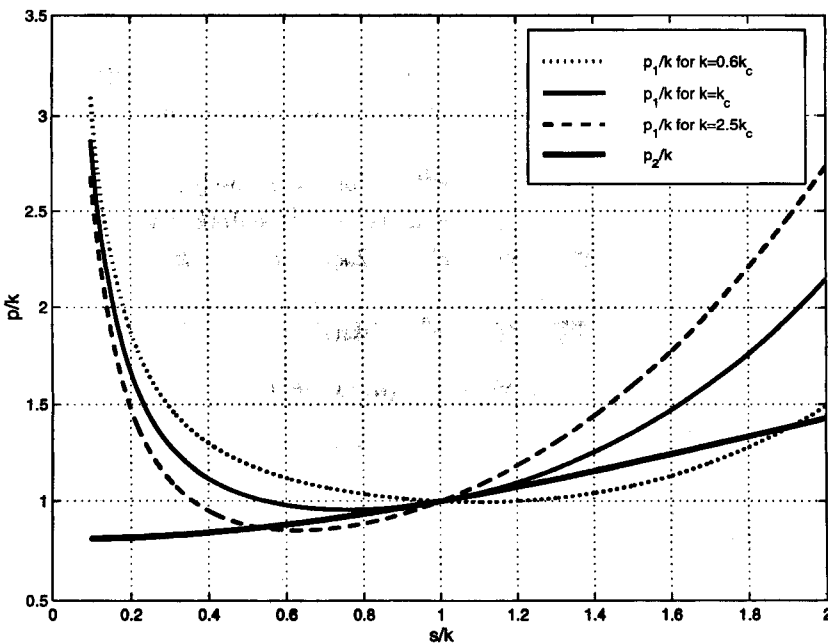

Figure C1.   The functions $\bar{p}_2(\bar{s})$ and $\bar{p}_1(\bar{s})$ for different values of k. The analysis of these functions give the proof of the existence of the cut off at k_c in the dominant part.

$$\bar{p} = \frac{(1 + \bar{s}^2)^2 - \bar{\alpha}_c \bar{s}(\bar{s}^2 - 1)}{4\bar{s}} = \bar{p}_1(\bar{s}), \quad \text{(C1)}$$

$$\bar{p} = \frac{1}{\eta}\sqrt{(\eta^2 - 1) + \bar{s}^2} = \bar{p}_2(\bar{s}). \quad \text{(C2)}$$

We want to solve for $\bar{s}$ that satisfies $\bar{p}_1(\bar{s}) = \bar{p}_2(\bar{s})$. One can verify that $\bar{s}_1 = 1$ is always a solution of systems (C1) and (C2). In this case, $\lambda = 0$. Moreover, the variations of the curves $\bar{p}_1(\bar{s})$ and $\bar{p}_2(\bar{s})$ indicate that there exist one other solution $\bar{s}_2$ (see Fig. C1). If $(d\bar{p}_1/d\bar{s})(\bar{s}_1) < (d\bar{p}_2/d\bar{s})(\bar{s}_1)$, then $\bar{s}_2 > 1$, and consequently, $\lambda(\bar{s}_2)$ is real. This condition is equivalent to $\bar{\alpha}_c > 2(1 - 1/\eta^2)$; that is, $k < k_c = \alpha_c/2(1 - 1/\eta^2)$. In other words, $k < k_c$ ensures that there is an $s > k$ so that λ is real and that there is a growing solution.

Appendix D

Dominant Eigenfunctions

Here we give the y-dependent functions Φ^k, Ψ^k, u_x^k, u_y^k, σ_{yy}^k, σ_{xy}^k, and σ_{xx}^k, for the dominant eigenfunctions.

$$\Phi^k(y) = 2ks(k)e^{-p(k)y},$$

$$\Psi^k(y) = [s^2(k) + k^2]e^{-s(k)y},$$

$$u_x^k(y) = s(k)\{-2k^2 e^{-p(k)y} + [s^2(k) + k^2]e^{-s(k)y}\},$$

$$u_y^k(y) = k\{-2p(k)s(k)e^{-p(k)y} + [s^2(k) + k^2]e^{-s(k)y}\},$$

$$\sigma_{xy}^k(y) = \rho v_s^2 \{4k^2 p(k)s(k)e^{-p(k)y} - [s^2(k) + k^2]^2 e^{-s(k)y}\},$$

$$\sigma_{yy}^k(y) = 2\rho v_s^2 ks(k)[s^2(k) + k^2][e^{-p(k)y} - e^{-s(k)y}],$$

$$\sigma_{xx}^k(y) = 2\rho v_s^2 ks(k)\{[s^2(k) - k^2 - 2p^2(k)]e^{-p(k)y} + [s^2(k) + k^2]e^{-s(k)y}\}.$$

Laboratoire de Géophysique Interne et Tectonophysique
Observatoire de Grenoble
Université Joseph Fourier
BP 53
38041 Grenoble Cedex 9, France
(P.F., M.C.)

Laboratoire de Mathématiques Appliquées
Université de Savoie
Campus Scientifique
73376 Le Bourget-du-lac
Cedex, France
(I.R.I.)